D. Delforge[1,2], O. de Viron[1], F. Durand[3,4] and V. Dehant[2]

[1]Littoral, Environnement et Sociétés, Université de La Rochelle and CNRS (UMR7266), La Rochelle, France.

[2]Royal Observatory of Belgium, Brussels, Belgium

[3]LEGOS (UMR5566), CNRS/CNES/IRD/UPS, Toulouse, France

[4]University of Brasilia (UnB), Institute of Geosciences, Brasilia, Brazil

Corresponding author: Damien Delforge (`damien.delforge@uclouvain.be`) †

†current addresses.

Key Points:

- The GRACE dataset is decomposed into 23 spatiotemporal patterns using Principal Component Analysis and the Varimax rotation;
- 13 patterns are significantly correlated to the wind stress curl and are located in areas where gravity anomalies were already documented;
- The other 10 are typically tropical and related to spatially coherent mass variations that deserve further study.

Abstract

We decompose the monthly global Ocean Bottom Pressure (OBP) from GRACE(-FO) mass concentration solutions, with trends and seasonal harmonics removed from the signal, to extract 23 significant regional modes of variability. The 23 modes are analyzed and discussed considering Sea-Level Anomalies (SLA), Wind Stress Curl (WSC), and major climate indices. Two-thirds of the patterns correspond to extratropical regions and are substantially documented in other global or regional studies. Over the equatorial band, the identified modes are unprecedented, with an amplitude ranging between 0.5 and 1 centimeter. With smaller amplitude than extratropical patterns, they appear to be less correlated with the local SLA or WSC; yet, they present significantly coherent dynamics. The Pacific Ocean modes show significant correlations with the Pacific Decadal Oscillation (PDO) and El Niño Southern Oscillation (ENSO).

Plain Language Summary

In the oceans, water mass may vary due to the hydrological cycle, its modification resulting from climate change, or astrophysical cycles influencing the Earth system resulting in phenomena like tides or annual/semi-annual cycles of mass variations. Apart from trends and cyclic variations, water mass variations in the ocean are less known except at the poles and at the middle or high latitudes, where they are often associated with the gyratory effect from winds interacting with the ocean bottom topography. This study analyzes the monthly water mass variations between 2002 and 2020 measured by the GRACE mission satellites over the global ocean without trends and cycles. Our method highlights the regional areas where a coherent dynamic behavior is observed over the global ocean. These consistent patterns are compared to the dynamics of sea-level variations, winds, and well-known indices associated with climate dynamics. In doing so, we recover known patterns from high and mid-latitudes but also other patterns from lower latitudes that are poorly documented in the scientific literature and would benefit from further study. In the Pacific, these patterns are associated with the climate phenomenon known as the El Niño-Southern Oscillation.

1 Introduction

Since 2002, the Gravity Recovery and Climate Experiment (GRACE) and its successor GRACE Follow-On (GRACE-FO) satellite missions allow monthly estimations of ocean mass distributions at the global scale, with a 3°×3° spatial resolution (Landerer et al., 2020; Tapley et al., 2004). GRACE products show a sensitivity at the subcentimetric level when expressed in equivalent water height (Chambers, 2006; Chambers et al., 2004). Besides GRACE(-FO), oceanic mass distributions are estimated through a limited set of Ocean Bottom Pressure (OBP) in-situ sensors, or from sea-level variations, indirectly, by removing steric effects (Chambers et al., 2004), or using Ocean General Circulation Models (OGCMs). Yet, OGCMs and GRACE(-FO) products have co-evolved along with our understanding of the global ocean. OGCMs offer opportunities of correcting GRACE(-FO) solutions from aliasing errors (Dobslaw et al., 2017; S. Han et al., 2004; Quinn & Ponte, 2011). The physical representativeness of GRACE(-FO) product over oceans was acknowledged early on (Chambers, 2006), even more today with recent mass concentration solutions better matching with in-situ OBP sensors (Piecuch et al., 2018; Save et al., 2016; Watkins et al., 2015). Conversely, empirical analyses of GRACE(-FO) products, or their assimilation in OGCMs, offer the opportunity of improving our understanding and model representation of the global ocean functioning (e.g., Chambers & Willis, 2008; Fukumori et al., 2021; Köhl et al., 2012).

Our study is part of this empirical process of understanding and targets the global detection of regionally consistent spatiotemporal patterns within the GRACE(-FO) data. In the literature, such global studies often consist of global sea-level budgets and comparisons with other models or datasets (Cazenave et al., 2018; Cheng et al., 2021; Humphrey et al., 2016; Johnson & Chambers, 2013; Kanzow et al., 2005; Ponte et al., 2007). Besides, except for some studies focusing on interannual or intraseasonal variations (Piecuch et al., 2013; Quinn & Ponte, 2012), most of these global ocean studies focus on trends or seasonal cycles given the substantial variance attributed to these components alongside anthropic concerns about sea-level rise.

Still, there are reasons to expect relevant signals and processes at interannual and intraseasonal time scales. Regarding processes, the mass distribution in the ocean is governed by the hydrostatic equilibrium, which implies that OBP reflects the mass of the ocean-atmosphere fluid column. The effect of the atmosphere tends to cancel out at timescales longer than a few days (Ponte, 1994).

Oceanic barotropic signals are supposed to be prominently related to high frequencies (Gill & Niller, 1973; Quinn & Ponte, 2012; Willebrand et al., 1980) but were also reported at intraseasonal (Afroosa et al., 2021; Rohith et al., 2019) and interannual scales (Piecuch et al., 2013). Besides land-ocean transfers, the ocean circulation, mass, and sea-level variations result from water density gradients or wind-driven Ekman transport (Stammer et al., 2013). Especially at mid-high latitudes such as in the southern ocean (Bingham & Hughes, 2008; Piecuch et al., 2013; Quinn & Ponte, 2012; Vinogradova et al., 2007), regional-scale sea-level variations mostly correspond to barotropic, i.e., depth-independent, wind-driven mass variations (Fu & Davidson, 1995). At lower latitudes, OBP variations potentially have a baroclinic contribution, typically at the subcentimetric level (Piecuch et al., 2015). However, instances of regional-scale barotropic sea-level variability were reported (Afroosa et al., 2021; Piecuch et al., 2015; Rohith et al., 2019; Willebrand et al., 1980). Climate dynamics also impact sea level and mass variation whatsoever the triggered mechanism (Hamlington et al., 2020; W. Han et al., 2017). Patterns of OBP variability are often related to climatic modes, especially the El Niño–Southern Oscillation (ENSO) in the Pacific (e.g., Chambers, 2011; Volkov et al., 2017).

Hence, by investigating GRACE(-FO) beyond seasonality and trends, we expect to reveal less understood patterns that would remain hidden otherwise and relate them to the above-mentioned processes discussed in regional studies. Our decomposition method for identifying patterns in interannual and intraseasonal GRACE(-FO) signals is based on Principal Component Analysis (PCA), also known as Empirical Orthogonal Functions (EOF) (von Storch & Zwiers, 1999). This method was applied in regional GRACE(-FO) study cases (Chambers & Willis, 2008; Liau & Chao, 2017; Piecuch et al., 2021; Wang et al., 2017) or globally as a collection of regional EOF (Marcos et al., 2011). Our approach differs as it is combined with a method to select the significant modes followed by a Varimax rotation (Kaiser, 1958; Vejmelka et al., 2015). As far as the dataset allows, the PCA-Varimax produces regionally concentrated patterns, thus comparable with regional case studies for further insights.

2 Data

2.1 GRACE(-FO) Data

We use JPL GRACE(-FO) RL06v02 mascons solution (DOI: 10.5067/TEMSC-3JC62, Watkins et al., 2015; Wiese et al., 2016) because of its fine representation of ocean dynamics. The trend, seasonal harmonics at the yearly and six-month periods, and the 161-days tidal alias resulting from S2 semidiurnal solar tide corrections (Chen et al., 2009) were subtracted by a least-squares fit. The time-domain covers 175 months from April 2002 to October 2020. Missing time-steps are those initially missing in the data or removed because of an incomplete and asymmetric sub-monthly coverage, as identified from the product metadata (Supplementary Table S1).

From the original 0.5°×0.5° grid, we sampled 10255 time-series over ocean area beyond 200 m depth, evenly distributed at the 16002 summits of an icosahedron. We removed areas affected by earthquakes above magnitude 8.8: Sumatra 2004, Chile 2010, and Japan 2011. Unrelated with ocean mass variation, earthquakes introduce sharp ruptures, the coseismic effect, and/or changes of trend, the postseismic effect, in the time-series (de Linage et al., 2009). Finally, time-series were standardized to have a zero mean and a unit standard deviation.

2.2 Co-related datasets: wind stress curl, sea level anomaly, and climate indices

The barotropic component of sea-level variability linearly responds to the Wind Stress Curl (WSC) under the assumption of quasi-geostrophic balance (Fu & Davidson, 1995). Wind data and Sea-Level Anomaly (SLA) were accessed through the Copernicus Climate Change Service (C3S). Both datasets were monthly averaged and coarsened from the $0.25°\times0.25°$ to the $0.5°\times0.5°$ grid of GRACE. Wind stress data are computed from ERA5 10 m zonal U and meridional V wind component (Hersbach et al., 2019). SLA is defined from multi-mission satellite altimetry as the deviation from the mean sea surface height from 1993-2012 (Taburet et al., 2019). The SLA dataset only covers the latitude range +/- 66 N°. The SLA and WSC time-series are five time-steps shorter than the GRACE(-FO) time-series due to the unavailability of the most recent time steps at the time of acquisition.

In addition, 42 climate indices were selected from the NOAA Physical Sciences Laboratory or Climate Prediction Center portals. The entire climate indices list is reported in the supplementary materials (Table S2). The main manuscript focuses on a smaller set of important indices being discussed: Arctic Oscillation (AO), Antarctic Oscillation (AAO), Multivariate ENSO Index version 2 (MEIv2), North Atlantic Oscillation (NAO), and Pacific Decadal Oscillation (PDO). For a consistent comparison, all time-series from the co-related datasets are processed with the same treatment as the GRACE(-FO) data (section 2.1).

3 Spatiotemporal pattern definition

Following Vejmelka et al. (2015), we identified GRACE-(FO) spatiotemporal patterns using rotated Principal Component Analysis (PCA-Varimax; Kaiser, 1958). PCA selects an orthogonal coordinate system of reduced dimensions capturing most of the variance of the data. This coordinate system is expressed in eigenvectors and eigenvalues, defining the axes' orientation and importance in terms of captured variance. Following PCA, the Varimax rotation tends to concentrate the energy on a minimum amount of time-series, i.e., to produce regionally concentrated patterns. In the end, PCA-Varimax components are associated with a spatial pattern and a time dimension as the original GRACE-(FO) dataset.

Regarding PCA, the number of coordinate axes or components is regularly set based on heuristic thresholds on the captured variance. Vejmelka et al. (2015)'s approach proposes an objective basis to define this number by comparison with random substitutes of the original dataset containing independent time-series. Such random substitutes, known as surrogates, are built to preserve some dynamical traits of the original dataset (Schreiber & Schmitz, 2000). In our case, the surrogate models result from autoregressive processes of order p (ARp), with p determined independently for each series to minimize the Bayesian Information Criterion (Schwarz, 1978), and the coefficient fit on the time-series using the Linear State-Space model framework (Durbin & Koopman, 2012; Seabold & Perktold, 2010).

4 Results

Figure 1 illustrates the selection of the number of principal components: Fig. 1a maps the distribution of the p orders of the surrogate models, while Fig. 1b shows the comparison between the GRACE(-FO) PCA eigenvalues and those from the decomposition of 100 surrogate datasets. The results led us to select 23 components (0 to 22), capturing together 72% of the original variance.

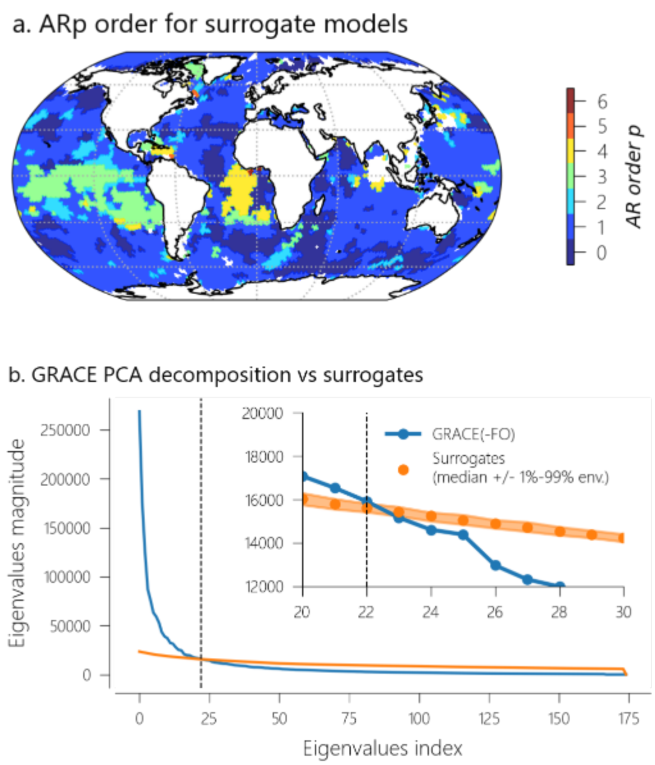

Figure 1. Selection of the 23 PCA components. (a) Order of the surrogates model (Eq. 1), and (b) Comparison of eigenvalues magnitude between the decomposition of GRACE(-FO) and the surrogate dataset.

Figure 2 displays the resulting 23 Varimax spatial patterns by showing the above-98$^{\text{th}}$ percentile filled contour of the load. Since it is a percentile, contours represent equal areas despite possible variations in the patterns' concentration.

For more details, spatial and temporal patterns are shown individually in the supplementary materials (Fig. S1, S2). The patterns' labels are centered on the maximum load location and ordered by decreasing percentages of captured variance in the standardized GRACE(-FO) dataset (CV_{std} column in Table 1). Providing that PCA-Varimax is applied on the standardized dataset, CV_{std} gives an estimate of the spatiotemporal importance of the identified dynamics regardless of their physical magnitude. From the CV_{std}'s perspective, the Western Equatorial Pacific pattern #0 is the most important, while pattern #22, over the Hudson and Baffin Bay, Labrador Sea, North Atlantic, and Mediterranean Sea, is the least significant.

Table 1 also displays $\text{LW}E_{\text{cov}}$ reflecting the importance of the patterns in mass variations (cm of liquid water equivalent or LWE). $\text{LW}E_{\text{cov}}$ is the average covariance between the standardized GRACE(-FO) PCA-Varimax temporal patterns (Fig. S2) and the original GRACE(-FO) time-series, without trends and seasonality, over the 98^{th} percentile envelope shown in Fig. 2. From that perspective, the Arctic pattern #12 is the most important, followed by the Australian-Antarctic pattern #11. Conversely, the intertropical Atlantic Pattern #1 and #9 are the least important in terms of mass deviations, despite their high captured variance in the normalized data set (CV_{std}).

The last two columns of Table 1, (#,SLA) and (#,WSC), report absolute values of Pearson's correlation coefficients between the GRACE(-FO) temporal pattern and the respective temporal projection of the SLA and WSC datasets (section 2.2). They indicate the coherence between the spatiotemporal pattern of mass variations for sea-level dynamics and the surface WSC. We tested the 99% significance by confronting the statistic to those obtained with 200 ARp surrogates of the GRACE(-FO) PCA-Varimax temporal pattern. In the supplementary materials, Fig. S3 and S4 show the spatial patterns of correlations for SLA and WSC, while Fig. S5 and S6 report the spatial patterns of correlations for zonal (τ_x) and meridional wind stress (τ_y).

Finally, Fig. 3 shows the result of the cross-correlation analysis for time lags between -12 and +12 months for the five selected climate indices: Arctic Oscillation (AO), Antarctic Oscillation (AAO), Multivariate ENSO Index version 2 (ENSO MEIv2), North Atlantic Oscillation (NAO), and Pacific Decadal Oscillation (PDO). More indices are tested in the supplements (Table S2 and Fig. S7). Below, Fig. 3b shows the auto-correlation of each PCA-Varimax GRACE-(FO) time-series. Results are presented in the form of cross-correlation clocks. In Fig. 3a, given the arrow of time, significant dependencies in the left quadrants denote a potential causal effect of the climate indices on the PCA-Varimax GRACE(-FO) patterns.

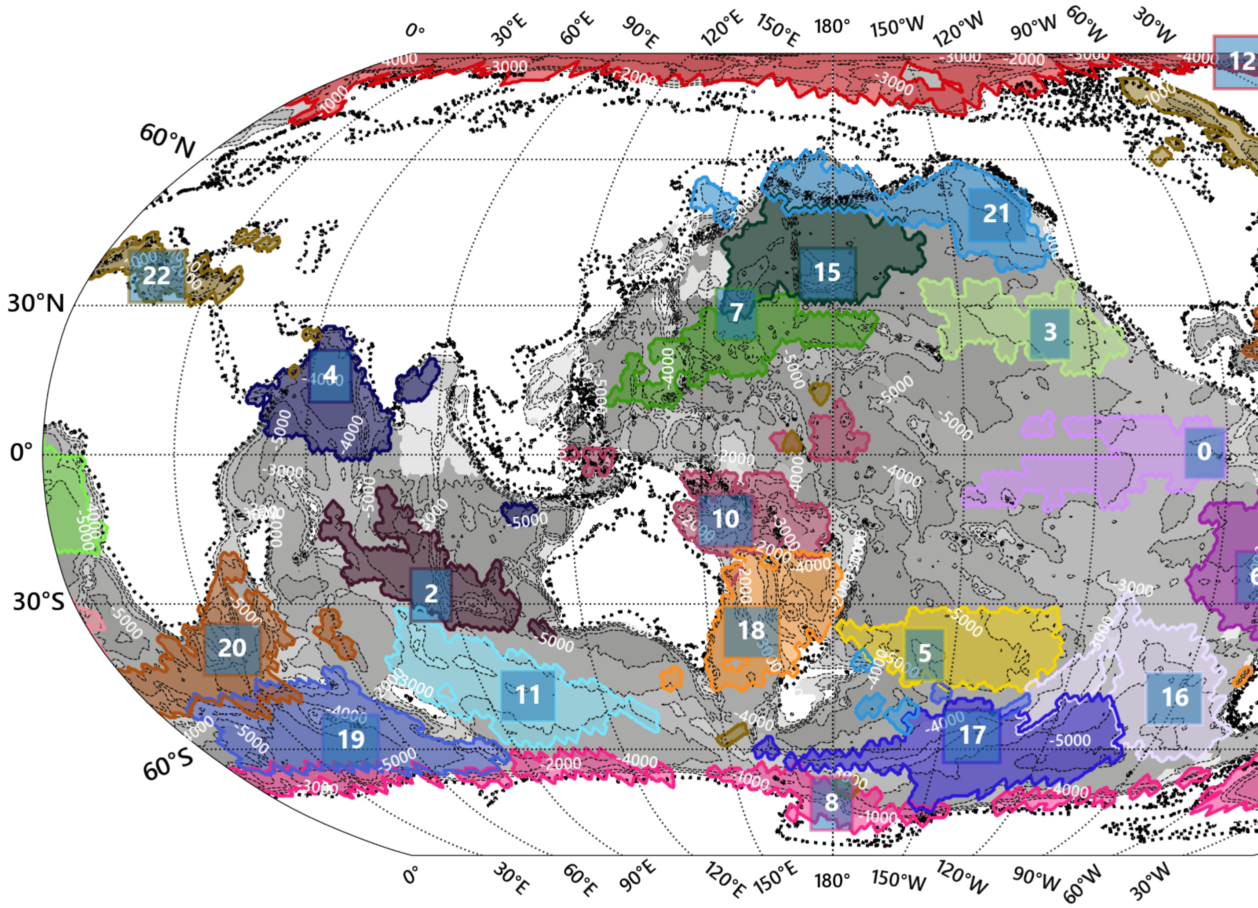

Figure 2. The 23 patterns obtained from the Varimax rotation of the PCA coordinate systems. Each pattern is sorted by decreasing captured variance and labeled accordingly from 0 to 22, with the label box located at the Varimax pattern's maximum concentration. The colored contour shows the extent of the area between 98% and the maximum. The gray background contours represent the ocean SRTM15+ bathymetry in meters (Tozer et al., 2019). White areas represent either land, shallow ocean (>-200m), or earthquake-impacted areas excluded from the analysis. The colormap was generated using *colorgorical* (Gramazio et al., 2017).

Table 1. Summary statistics and summary correlation statistics for the 23 PCA-Varimax patterns.

#	**Lat.**	LW$\mathbf{E}_{cov}$	$\mathbf{CV}_{std}$	$\lvert(\#,\ \mathbf{SLA})\rvert$	$\lvert(\#,\ \mathbf{WSC})\rvert$
	°N	cm	%	[0-1]	[0-1]
				0.39	
				0.40	**0.20**
				0.37	
					0.57
				0.36	
					0.26
				0.34*	**0.55**
				0.23	
				0.67	**0.69**
				0.58*	**0.49**
					0.35
					0.24
				0.40	**0.61**
				0.73	**0.38**
				0.71	**0.33**
				0.64	**0.70**
					0.30
				0.42	**0.26**

#	**Lat.** °N	LW$\mathbf{E}_{cov}$ cm	$\mathbf{CV}_{std}$ %	$\mid(\#,\ \mathbf{SLA})\mid$ [0-1]	$\mid(\#,\ \mathbf{WSC})\mid$ [0-1]

Legend
Lat: Latitude of the pattern based on Figure 2 label's position; LW$\mathbf{E}_{cov}$: Average covariance between the standardized GRACE-FO temporal pattern and the original GRACE(-FO) dataset over the 98th percentile envelope shown in Figure 2; $\mathbf{CV}_{std}$**:** Percentage of captured variance for the standardized GRACE(-FO) dataset; $\mid(\#,\ \mathbf{SLA})\mid$**:** Absolute Pearson's correlation coefficient between the GRACE(-FO) temporal pattern # and the

#	**Lat.**	LW**E**$_{cov}$	**CV**$_{std}$	| (#, **SLA**)|	| (#, **WSC**)|
	°N	cm	%	[0-1]	[0-1]

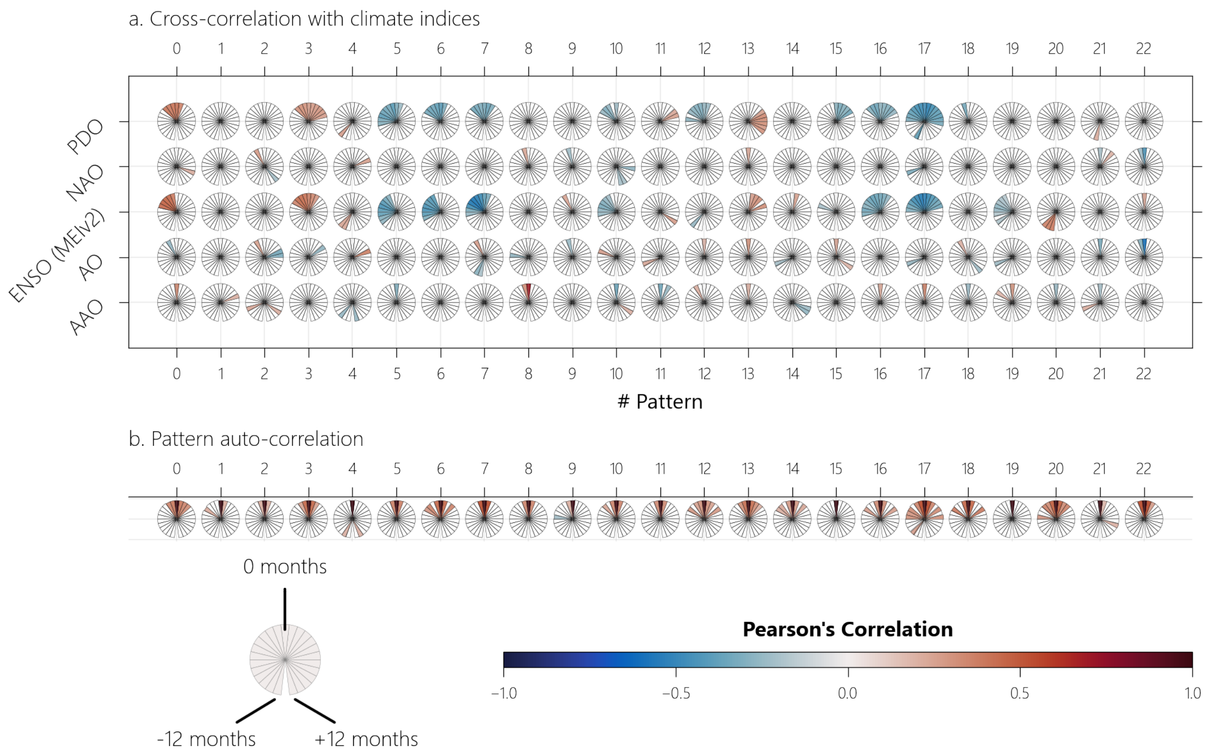

Figure 3. Cross-correlation analysis between the PCA-Varimax GRACE(-FO) patterns and (a) the climate indices Arctic Oscillation (AO), Antarctic Oscillation (AAO), Multivariate ENSO Index version 2 (ENSO MEIv2), North Atlantic Oscillation (NAO), and Pacific Decadal Oscillation (PDO); and (b) the auto-correlation of the pattern. The results are presented on 25-segments clocks. Only significant dependencies are colored, based on 200 ARp surrogates comparison. 12 o'clock indicates instantaneous correlation. The left quadrants relate to negative lags of the climate indices (a) or the pattern (b), counterclockwise down to -12 months. The right quadrants contain positive lags clockwise up to +12 months.

5 Discussion

Overall, the significant patterns show spatial consistency, often matching bathymetric contours (Fig. 2), or having their limits over bathymetric features, in line with the known ability of oceanic slopes to trap barotropic transients (e.g., Rohith et al., 2019). Yet, relationships with the SLA and WSC are not systematically significant (Table 1, $|\rho(\#, SLA)|$,$|\rho(\#, WSC)|$), whereas such a relation is expected from the literature (Fu & Davidson, 1995). This implies significant remote forcing of SLA by WSC, as already evidenced in some regions of the world Ocean (e.g., Afroosa et al., 2021; Rohith et al., 2019), and/or a prominent fraction of SLA variability that is baroclinic in nature. In Fig. 4, correlations between WSC and load patterns from Table 1 are plotted against latitude. The linear fit shows an overall poleward increase of correlation in both hemispheres, from insignificant values close to the equator to values above 0.2 at higher latitudes.

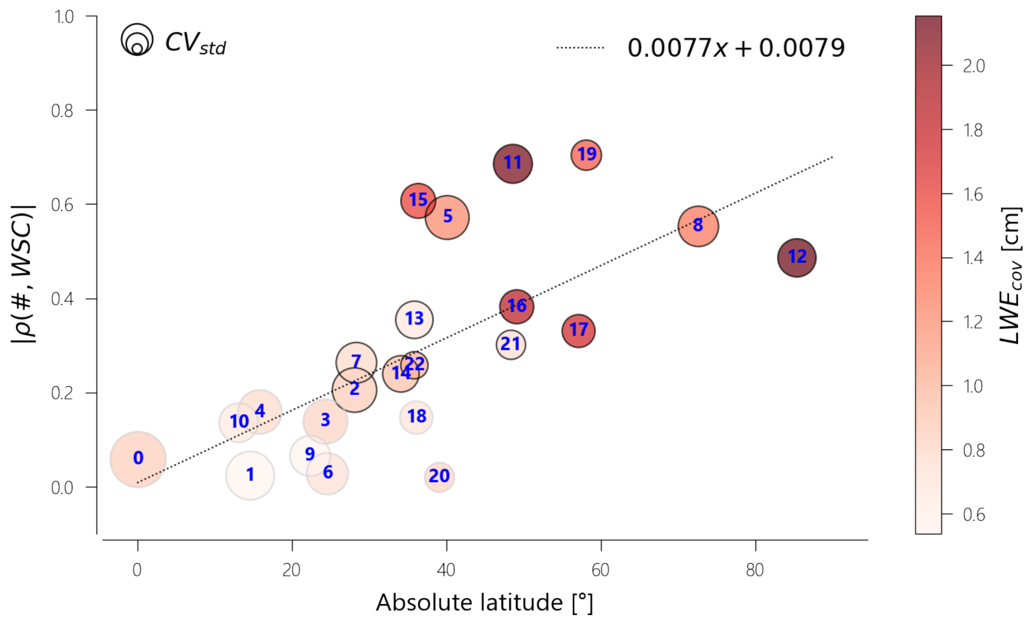

Figure 4. Graphical analysis of the statistics of Table 1. The correlation (#,WSC) between temporal PCA-Varimax GRACE(-FO) patterns and temporal projections of WSC onto the PCA-Varimax system is reported against the absolute latitude of spatial pattern maximum's concentration (Fig. 2). Markers with a black edge have a significant correlation. The markers' size and color respectively map to CV_{std} and LWE_{cov}. The pattern index from Fig. 2 is labeled in blue.

The mid-latitude patterns #11, #16, #17, and #19 in the Southern Ocean and #15 in the North Pacific Ocean echo to a highly significant driving by regional winds, associated with strong mass variations (LWE_{cov}) with a dominant high frequency (Fig. 3.b). Their load patterns concentrate at medium and high latitudes, as discussed in the literature (Piecuch et al., 2013, 2015; Quinn & Ponte, 2012).

At the North Pole, the high absolute variance Arctic pattern #12 owes its coherence to the semi-enclosed character of the Arctic Ocean and is wind-driven. It has been the subject of substantial literature (Fukumori et al., 2015; Peralta-Ferriz et al., 2014; Volkov & Landerer, 2013). In the Northern Atlantic, the Artic pattern is related to #22, as WSC plays an important role in the mass exchange among the Arctic and North Atlantic Ocean (Fukumori et al., 2015, and Fig. S4 to S6). This pattern #22 extends to the semi-enclosed Canadian lakes and the Mediterranean Sea. It was discussed in several studies about its link to NAO (Fig. 3) or the Atlantic Meridional Overturning Circulation (AMOC) (Fukumori et al., 2007; Piecuch & Ponte, 2015; Tsimplis et al., 2013; Volkov et al., 2019). It shows a smaller consistency (CV_{std}) in Table 1 and Fig. 4, probably due to its extensive and fragmented spatial distribution. To the South, pattern #13 appears to be driven by the wind stress and statistically related to the AMOC as well as to NAO and AO (Landerer et al., 2015; Piecuch & Ponte, 2014b, and Fig. 3).

In the North Pacific, patterns #12 and #21 are connected through the Bering Strait (Peralta-Ferriz & Woodgate, 2017; Volkov & Landerer, 2013). The subpolar pattern #15 was reported in previous studies focusing on interannual, annual, or seasonal scales (Bingham & Hughes, 2006; Chambers, 2011; Chambers & Willis, 2008; Song & Qu, 2011; Song & Zlotnicki, 2008). Accordingly, #15 would be coupled with pattern #7, which is forced by the ENSO-influenced northern subtropical Pacific gyre (Fig. 3). This same pattern #7 is an area of maxima in terms of dynamic topography subject to steep changes in sea level, with the mass component related to the variability of Easterlies (Fig. S5) and of the North Equatorial Current over decadal timescales (Moon & Song, 2013; Qiu & Chen, 2010; Timmermann et al., 2010), in phase with PDO (Cheng et al., 2013, and Fig. 3).

In the southern hemisphere, besides the afore-mentioned highly significant patterns (#11, #16, #17, and #19), the South Pacific Gyre pattern #5 correlates significantly with SLA and WSC (Table 1 and Fig S4 to S6). Together with the Indian Ocean (~#2), this area is exposed to heat uptake and decadal sea-level change where heat transfers are related to Ekman pumping (Llovel & Terray, 2016; Roemmich et al., 2016; Volkov et al., 2017). It is also associated with transport from the Antarctic Bottom Water into the Pacific Ocean (Mazloff & Boening, 2016; Volkov et al., 2017). The South Indian Ocean pattern (~#2) involves both barotropic and baroclinic processes at the annual scale (Piecuch & Ponte, 2014a). Other recent studies present further evidence of barotropic processes at intraseasonal timescale over the Indian Ocean (Afroosa et al., 2021; Manche et al., 2021; Rohith et al., 2019). In a region close to our pattern #14, a sea-level trend associated with the Atlantic subtropical gyre has been shown by Drouin et al. (2021) and Ruiz-Etcheverry & Saraceno (2020). The Antarctic Pattern #8 is driven by the zonal wind stress (Fig. S5.i) driving meridional Ekman transport and related to the AAO climate index (Ponte & Quinn, 2009, and Fig. 3). This pattern has been well documented and studied using the GRACE dataset (Feng et al., 2013; Liau & Chao, 2017; Ponte & Piecuch, 2014).

Despite their spatially significant dynamical consistency, the remaining ten patterns (#0 to #4, #6, #9, #10, #18, and #20) are not significantly associated with WSC based on our indicator (Table 1, Fig. 4), which does not mean that they are uncorrelated with the wind stress, as the correlation is often significant over remote regions located outside patterns' boundaries (see Fig. S4 to S6). They are also less documented in the literature. Still, Pattern #20, corresponding to the eddy-influenced area of the Agulhas current, is discussed in Kuhlmann et al. (2013), whereas patterns #10 and #18 correspond to the Coral Sea and the Tasman Sea, both bordered by steep bathymetric features to the East and the North, and known to be influenced by remote WSC from the Maritime Continent at intra-seasonal timescales (Afroosa et al., 2021). The mechanisms of patterns #0, #3, and #6 remain unclear and may be related to the barotropic response of OBP to remote WSC. They show long memory and are related to ENSO (MEIv2) or PDO (Fig. 3). Besides, these patterns may not be physically large enough (LWE_{cov}) to allow identification of significant correlations with WSC and SLA, especially for the weakest ones in the Equatorial Atlantic (#1, #9). Possibly, a part of the OBP response in GRACE(-FO) could be baroclinic but this phenomenon should be marginal (<0.4 cm) and mostly annual (Piecuch, 2013, 2015; Piecuch et al., 2015; Piecuch & Ponte, 2014a).

6 Conclusions

We have shown that the spatiotemporal decomposition method, Principal Component Analysis followed by a Varimax rotation (PCA-Varimax), can objectively evidence in a global analysis the GRACE(-FO) patterns that are usually extracted by Empirical Orthogonal Function (EOF) or PCA alone within arbitrary regional bounding boxes. The resulting 23 significant interannual and intraseasonal GRACE(-FO) patterns are spatially coherent and scattered over the global ocean, with mass deviations ranging between 0.54 cm and 2.15 cm. Thirteen of them significantly relate to wind stress curl and echo to barotropic OBP variations documented in the literature. Conversely, the remaining ten patterns are mainly intertropical and are less documented in the published literature, although our analysis shows that they represent coherent dynamical modes with centimetric mass signatures. Those in the Pacific Ocean are mainly related to the Pacific Decadal Oscillation (PDO) and El Niño Southern Oscillation (ENSO). In addition to this empirical analysis, the patterns we have identified would benefit from being studied from a mechanistic perspective, e.g., relying on Ocean Global Circulation Models. In this sense, these particular patterns call for dedicated ocean modeling investigations.

Acknowledgments

Damien Delforge is supported by the Centre National d'Études Spatiales (CNES, France) through a post-doctoral grant. V. Dehant has received funding from the European Research Council (ERC) under the European Union's Horizon 2020 research and innovation programme (GRACEFUL Synergy Grant agreement No 855677).

Open research

GRACE/GRACE-FO Mascon data are available at http://grace.jpl.nasa.gov. Wind data from ERA5 (Hersbach et al., 2019) and Sea Surface Anomaly data (Taburet et al., 2019) were acquired from Copernicus Climate Change Service (C3S) portal (cds.climate.copernicus.eu). Climate Indices data can be downloaded from the following links on the NOAA portal: Arctic Oscillation (psl.noaa.gov/data/correlation/ao.data), Antarctic Oscillation (psl.noaa.gov/data/correlation/aao.data), Multivariate ENSO Index (psl.noaa.gov/enso/mei/data/meiv2.data), North Atlantic Oscillation (psl.noaa.gov/data/correlation/nao.data), and Pacific Decadal Oscillation (psl.noaa.gov/data/correlation/pdo.data).

The analysis was conducted using Python: the scikit-learn package for PCA and the Varimax rotation (Pedregosa et al., 2011), and the statmodels package for Autoregressive Model fitting, and surrogate data generation (Durbin & Koopman, 2012; Seabold & Perktold, 2010).

References

Afroosa, M., Rohith, B., Paul, A., Durand, F., Bourdallé-Badie, R., Sreedevi, P. V., et al. (2021). Madden-Julian oscillation winds excite an intraseasonal see-saw of ocean mass that affects Earth's polar motion. *Communications Earth & Environment*, *2*(1), 1–8. https://doi.org/10.1038/s43247-021-00210-xBingham, R. J., & Hughes, C. W. (2006). Observing seasonal bottom pressure variability in the North Pacific with GRACE. *Geophysical Research Letters*, *33*(8). https://doi.org/10.1029/2005GL025489Bingham, R. J., & Hughes, C. W. (2008). The relationship between sea-level and bottom pressure variability in an eddy permitting ocean model. *Geophysical Research Letters*, *35*(3). https://doi.org/10.1029/2007GL032662Cazenave, A., Palanisamy, H., & Ablain, M. (2018). Contemporary sea level changes from satellite altimetry: What have we learned? What are the new challenges? *Advances in Space Research*, *62*(7), 1639–1653. https://doi.org/10.1016/j.asr.2018.07.017Chambers, D. P. (2006). Evaluation of new GRACE time-variable gravity data over the ocean. *Geophysical Research Letters*, *33*(17). https://doi.org/10.1029/2006GL027296Chambers, D. P. (2011). ENSO-correlated fluctuations in ocean bottom pressure and wind-stress curl in the North Pacific. *Ocean Science*, *7*(5), 685–692. https://doi.org/10.5194/os-7-685-2011Chambers, D. P., & Willis, J. K. (2008). Analysis of large-scale ocean bottom pressure variability in the North Pacific. *Journal of Geophysical Research: Oceans*, *113*(C11). https://doi.org/10.1029/2008JC004930Chambers, D. P., Wahr, J., & Nerem, R. S. (2004). Preliminary observations of global ocean mass variations with GRACE. *Geophysical Research Letters*, *31*(13). https://doi.org/10.1029/2004GL020461Chen, J. L., Wilson, C. R., & Seo, K. (2009). S2 tide aliasing in GRACE time-variable gravity solutions. *Journal of Geodesy*, *83*(7), 679–687. https://doi.org/10.1007/s00190-008-0282-1Cheng, X., Li, L., Du, Y., Wang, J., & Huang, R. (2013). Mass-induced sea level change in the northwestern North Pacific and its contribution to total sea level change. *Geophysical Research Letters*, *40*(15), 3975–3980. https://doi.org/10.1002/grl.50748Cheng, X., Ou, N., Chen, J., & Huang, R. X. (2021). On the seasonal variations of ocean bottom pressure in the world oceans. *Geoscience Letters*, *8*(1), 29. https://doi.org/10.1186/s40562-021-00199-3Dobslaw, H., Bergmann-Wolf, I., Dill, R., Poropat, L., Thomas, M., Dahle, C., et al. (2017). A new high-resolution model of non-tidal atmosphere and ocean mass variability for de-aliasing of satellite gravity observations: AOD1B RL06. *Geophysical Journal International*, *211*(1), 263–269. https://doi.org/10.1093/gji/ggx302Drouin, K. L., Lozier, M. S., & Johns, W. E. (2021). Variability and Trends of the South Atlantic Subtropical Gyre. *Journal of Geophysical Research: Oceans*, *126*(1), e2020JC016405. https://doi.org/10.1029/2020JC016405Durbin, J., & Koopman, S. J. (2012). *Time series analysis by state space methods* (2nd ed). Oxford: Oxford University Press.Feng, G., Jin, S., & Reales, J. M. S. (2013). Antarctic circumpolar current from satellite gravimetric models ITG-GRACE2010, GOCE-TIM3 and satellite altimetry. *Journal of Geodynamics*, *72*, 72–80. https://doi.org/10.1016/j.jog.2013.08.005Fu, L.-L., & Davidson, R. A. (1995). A note on the barotropic response of sea level to time-dependent wind forcing. *Journal of Geophysical Research*, *100*(C12), 24955. https://doi.org/10.1029/95JC02259Fukumori, I., Menemenlis, D., & Lee, T. (2007). A Near-Uniform Basin-Wide Sea Level Fluctuation of the Mediterranean Sea. *Journal of Physical Oceanography*, *37*(2), 338–358. https://doi.org/10.1175/JPO3016.1Fukumori, I., Wang, O., Llovel, W., Fenty, I., & Forget, G. (2015). A near-uniform fluctuation of ocean bottom pressure and sea level across the deep ocean basins of the Arctic Ocean and the Nordic Seas. *Progress in Oceanography*, *134*, 152–172. https://doi.org/10.1016/j.pocean.2015.01.013Fukumori, I., Wang, O., Fenty, I., Forget, G., Heimbach, P., & Ponte, R. M. (2021). *Synopsis of the ECCO Central Production Global Ocean and Sea-Ice State Estimate, Version 4 Release 4* (Version 4 Release 4). ECCO Consortium. https://doi.org/10.5281/ZENODO.4533349Gill, A. E., & Niller, P. P. (1973). The theory of the seasonal variability in the ocean. *Deep Sea Research and Oceanographic Abstracts*, *20*(2), 141–177. https://doi.org/10.1016/0011-7471(73)90049-1Gramazio, C. C., Laidlaw, D. H., & Schloss, K. B. (2017). Colorgorical: Creating discriminable and preferable color palettes for information visualization. *IEEE Transactions on Visualization and Computer Graphics*, *23*(1), 521–530. https://doi.org/10.1109/TVCG.2016.2598918Hamlington, B. D., Piecuch, C. G., Reager, J. T., Chandanpurkar, H., Frederikse, T., Nerem, R. S., et al. (2020). Origin of interannual variability in global mean sea level. *Proceedings of the National Academy of Sciences*, *117*(25), 13983–13990. https://doi.org/10.1073/pnas.1922190117Han, S., Jekeli, C., & Shum, C. K. (2004). Time-variable aliasing effects of ocean tides, atmosphere, and continental water mass on monthly mean GRACE gravity field. *Journal of Geophysical Research: Solid Earth*, *109*(B4). https://doi.org/10.1029/2003JB002501Han, W., Meehl, G. A., Stammer, D., Hu, A., Hamlington, B., Kenigson, J., et al. (2017). Spatial Patterns of Sea Level Variability Associated with

Natural Internal Climate Modes. In A. Cazenave, N. Champollion, F. Paul, & J. Benveniste (Eds.), *Integrative Study of the Mean Sea Level and Its Components* (pp. 221–254). Cham: Springer International Publishing. https://doi.org/10.1007/978-3-319-56490-6_10Hersbach, H., Bell, B., Berrisford, P., Biavati, G., Horányi, A., Muñoz Sabater, J., et al. (2019). ERA5 monthly averaged data on single levels from 1979 to present. Copernicus Climate Change Service (C3S) Climate Data Store (CDS). Retrieved from https://doi.org/10.24381/cds.6860a573Humphrey, V., Gudmundsson, L., & Seneviratne, S. I. (2016). Assessing Global Water Storage Variability from GRACE: Trends, Seasonal Cycle, Subseasonal Anomalies and Extremes. *Surveys in Geophysics*, *37*(2), 357–395. https://doi.org/10.1007/s10712-016-9367-1Johnson, G. C., & Chambers, D. P. (2013). Ocean bottom pressure seasonal cycles and decadal trends from GRACE Release-05: Ocean circulation implications. *Journal of Geophysical Research: Oceans*, *118*(9), 4228–4240. https://doi.org/10.1002/jgrc.20307Kaiser, H. F. (1958). The varimax criterion for analytic rotation in factor analysis. *Psychometrika*, *23*(3), 187–200. https://doi.org/10.1007/BF02289233Kanzow, T., Flechtner, F., Chave, A., Schmidt, R., Schwintzer, P., & Send, U. (2005). Seasonal variation of ocean bottom pressure derived from Gravity Recovery and Climate Experiment (GRACE): Local validation and global patterns. *Journal of Geophysical Research: Oceans*, *110*(C9). https://doi.org/10.1029/2004JC002772Köhl, A., Siegismund, F., & Stammer, D. (2012). Impact of assimilating bottom pressure anomalies from GRACE on ocean circulation estimates. *Journal of Geophysical Research: Oceans*, *117*(C4). https://doi.org/10.1029/2011JC007623Kuhlmann, J., Dobslaw, H., Petrick, C., & Thomas, M. (2013). Ocean bottom pressure signals around Southern Africa from in situ measurements, satellite data, and modeling. *Journal of Geophysical Research: Oceans*, *118*(10), 4889–4898. https://doi.org/10.1002/jgrc.20372Landerer, F. W., Wiese, D. N., Bentel, K., Boening, C., & Watkins, M. M. (2015). North Atlantic meridional overturning circulation variations from GRACE ocean bottom pressure anomalies. *Geophysical Research Letters*, *42*(19), 8114–8121. https://doi.org/10.1002/2015GL065730Landerer, F. W., Flechtner, F. M., Save, H., Webb, F. H., Bandikova, T., Bertiger, W. I., et al. (2020). Extending the Global Mass Change Data Record: GRACE Follow-On Instrument and Science Data Performance. *Geophysical Research Letters*, *47*(12), e2020GL088306. https://doi.org/10.1029/2020GL088306Liau, J., & Chao, B. F. (2017). Variation of Antarctic circumpolar current and its intensification in relation to the southern annular mode detected in the time-variable gravity signals by GRACE satellite. *Earth, Planets and Space*, *69*(1), 93. https://doi.org/10.1186/s40623-017-0678-3de Linage, C., Rivera, L., Hinderer, J., Boy, J.-P., Rogister, Y., Lambotte, S., & Biancale, R. (2009). Separation of coseismic and postseismic gravity changes for the 2004 Sumatra-Andaman earthquake from 4.6 yr of GRACE observations and modelling of the coseismic change by normal-modes summation. *Geophysical Journal International*, *176*(3), 695–714. https://doi.org/10.1111/j.1365-246X.2008.04025.xLlovel, W., & Terray, L. (2016). Observed southern upper-ocean warming over 2005–2014 and associated mechanisms, *11*(12), 124023. https://doi.org/10.1088/1748-9326/11/12/124023Manche, S. S., Nayak, R. K., Mohanty, P. C., Shesasai, M. V. R., & Dadhwal, V. K. (2021). Assessment of mass-induced sea level variability in the Tropical Indian Ocean based on GRACE and altimeter observations. *Journal of Geodesy*, *95*(2), 19. https://doi.org/10.1007/s00190-021-01471-2Marcos, M., Calafat, F. M., Llovel, W., Gomis, D., & Meyssignac, B. (2011). Regional distribution of steric and mass contributions to sea level changes. *Global and Planetary Change*, *76*(3), 206–218. https://doi.org/10.1016/j.gloplacha.2011.01.007Mazloff, M. R., & Boening, C. (2016). Rapid variability of Antarctic Bottom Water transport into the Pacific Ocean inferred from GRACE. *Geophysical Research Letters*, *43*(8), 3822–3829. https://doi.org/10.1002/2016GL068474Moon, J., & Song, Y. T. (2013). Sea level and heat content changes in the western North Pacific. *Journal of Geophysical Research: Oceans*, *118*(4), 2014–2022. https://doi.org/10.1002/jgrc.20096Pedregosa, F., Varoquaux, G., Gramfort, A., Michel, V., Thirion, B., Grisel, O., et al. (2011). Scikit-learn: Machine Learning in Python. *Journal of Machine Learning Research*, *12*, 2825–2830.Peralta-Ferriz, C., & Woodgate, R. A. (2017). The Dominant Role of the East Siberian Sea in Driving the Oceanic Flow Through the Bering Strait—Conclusions From GRACE Ocean Mass Satellite Data and In Situ Mooring Observations Between 2002 and 2016. *Geophysical Research Letters*, *44*(22), 11,472-11,481. https://doi.org/10.1002/2017GL075179Peralta-Ferriz, C., Morison, J. H., Wallace, J. M., Bonin, J. A., & Zhang, J. (2014). Arctic Ocean Circulation Patterns Revealed by GRACE. *Journal of Climate*, *27*(4), 1445–1468. https://doi.org/10.1175/JCLI-D-13-00013.1Piecuch, C. G. (2013). Dynamics of satellite-derived interannual ocean bottom pressure variability in the western tropical North Pacific. *Journal of Geophysical Research: Oceans*, *118*(10), 5117–5128. https://doi.org/10.1002/jgrc.20374Piecuch, C. G. (2015). Bottom-pressure signature of annual baroclinic Rossby waves in the northeast tropical Pacific Ocean. *Journal of Geophysical Research: Oceans*, *120*(4), 2449–2459. https://doi.org/10.1002/2014JC010667Piecuch, C. G., & Ponte, R. M. (2014a). Annual Cycle in Southern Tropical Indian Ocean Bottom Pressure. *Journal of Physical Oceanography*, *44*(6), 1605–1613. https://doi.org/10.1175/JPO-D-13-0277.1Piecuch, C. G., & Ponte, R. M. (2014b). Nonseasonal mass fluctuations in the midlatitude North Atlantic Ocean. *Geophysical Research Letters*, *41*(12), 4261–4269. https://doi.org/10.1002/2014GL060248Piecuch, C. G., & Ponte, R. M. (2015). A wind-driven nonseasonal barotropic fluctuation of the Canadian inland seas. *Ocean Science*, *11*(1), 175–185. https://doi.org/10.5194/os-11-175-2015Piecuch, C. G., Quinn, K. J., & Ponte, R. M. (2013). Satellite-derived interannual ocean bottom pressure variability and its relation to sea level. *Geophysical Research Letters*, *40*(12), 3106–3110. https://doi.org/10.1002/grl.50549Piecuch, C. G., Fukumori, I., Ponte, R. M., & Wang, O. (2015). Vertical Structure of Ocean Pressure Variations with Application to Satellite-Gravimetric Observations. *Journal of Atmospheric and Oceanic Technology*, *32*(3), 603–613. https://doi.org/10.1175/JTECH-D-14-00156.1Piecuch, C. G., Landerer, F. W.,

& Ponte, R. M. (2018). Tide gauge records reveal improved processing of gravity recovery and climate experiment time-variable mass solutions over the coastal ocean. *Geophysical Journal International*, *214*(2), 1401–1412. https://doi.org/10.1093/gji/ggy207Piecuch, C. G., Fukumori, I., & Ponte, R. M. (2021). Intraseasonal Sea Level Variability in the Persian Gulf. *Journal of Physical Oceanography*, *51*(5), 1687–1704. https://doi.org/10.1175/JPO-D-20-0296.1Ponte, R. M. (1994). Understanding the relation between wind- and pressure-driven sea level variability. *Journal of Geophysical Research: Oceans*, *99*(C4), 8033–8039. https://doi.org/10.1029/94JC00217Ponte, R. M., & Piecuch, C. G. (2014). Interannual Bottom Pressure Signals in the Australian–Antarctic and Bellingshausen Basins. *Journal of Physical Oceanography*, *44*(5), 1456–1465. https://doi.org/10.1175/JPO-D-13-0223.1Ponte, R. M., & Quinn, K. J. (2009). Bottom pressure changes around Antarctica and wind-driven meridional flows. *Geophysical Research Letters*, *36*(13). https://doi.org/10.1029/2009GL039060Ponte, R. M., Quinn, K. J., Wunsch, C., & Heimbach, P. (2007). A comparison of model and GRACE estimates of the large-scale seasonal cycle in ocean bottom pressure. *Geophysical Research Letters*, *34*(9). https://doi.org/10.1029/2007GL029599Qiu, B., & Chen, S. (2010). Interannual-to-Decadal Variability in the Bifurcation of the North Equatorial Current off the Philippines. *Journal of Physical Oceanography*, *40*(11), 2525–2538. https://doi.org/10.1175/2010JPO4462.1Quinn, K. J., & Ponte, R. M. (2011). Estimating high frequency ocean bottom pressure variability. *Geophysical Research Letters*, *38*(8). https://doi.org/10.1029/2010GL046537Quinn, K. J., & Ponte, R. M. (2012). High frequency barotropic ocean variability observed by GRACE and satellite altimetry. *Geophysical Research Letters*, *39*(7). https://doi.org/10.1029/2012GL051301Roemmich, D., Gilson, J., Sutton, P., & Zilberman, N. (2016). Multidecadal Change of the South Pacific Gyre Circulation. *Journal of Physical Oceanography*, *46*(6), 1871–1883. https://doi.org/10.1175/JPO-D-15-0237.1Rohith, B., Paul, A., Durand, F., Testut, L., Prerna, S., Afroosa, M., et al. (2019). Basin-wide sea level coherency in the tropical Indian Ocean driven by Madden–Julian Oscillation. *Nature Communications*, *10*(1), 1257. https://doi.org/10.1038/s41467-019-09243-5Ruiz-Etcheverry, L. A., & Saraceno, M. (2020). Sea Level Trend and Fronts in the South Atlantic Ocean. *Geosciences*, *10*(6), 218. https://doi.org/10.3390/geosciences10060218Save, H., Bettadpur, S., & Tapley, B. D. (2016). High-resolution CSR GRACE RL05 mascons. *Journal of Geophysical Research: Solid Earth*, *121*(10), 7547–7569. https://doi.org/10.1002/2016JB013007Schreiber, T., & Schmitz, A. (2000). Surrogate time series. *Physica D: Nonlinear Phenomena*, *142*(3), 346–382. https://doi.org/10.1016/S0167-2789(00)00043-9Schwarz, G. (1978). Estimating the Dimension of a Model. *The Annals of Statistics*, *6*(2), 461–464. https://doi.org/10.1214/aos/1176344136Seabold, S., & Perktold, J. (2010). Statsmodels: Econometric and Statistical Modeling with Python (pp. 92–96). Presented at the Python in Science Conference, Austin, Texas. https://doi.org/10.25080/Majora-92bf1922-011Song, Y. T., & Qu, T. (2011). Multiple Satellite Missions Confirming the Theory of Seasonal Oceanic Variability in the Northern North Pacific. *Marine Geodesy*, *34*(3–4), 477–490. https://doi.org/10.1080/01490419.2011.590110Song, Y. T., & Zlotnicki, V. (2008). Subpolar ocean bottom pressure oscillation and its links to the tropical ENSO. *International Journal of Remote Sensing*, *29*(21), 6091–6107. https://doi.org/10.1080/01431160802175538Stammer, D., Cazenave, A., Ponte, R. M., & Tamisiea, M. E. (2013). Causes for Contemporary Regional Sea Level Changes. *Annual Review of Marine Science*, *5*(1), 21–46. https://doi.org/10.1146/annurev-marine-121211-172406von Storch, H., & Zwiers, F. W. (1999). *Statistical Analysis in Climate Research*. Cambridge University Press. https://doi.org/10.1017/CBO9780511612336Taburet, G., Sanchez-Roman, A., Ballarotta, M., Pujol, M., Legeais, J., Fournier, F., et al. (2019). DUACS DT2018: 25 years of reprocessed sea level altimetry products. *Ocean Science*, *15*(5), 1207–1224. https://doi.org/10.5194/os-15-1207-2019Tapley, B. D., Bettadpur, S., Watkins, M., & Reigber, C. (2004). The gravity recovery and climate experiment: Mission overview and early results. *Geophysical Research Letters*, *31*(9). https://doi.org/10.1029/2004GL019920Timmermann, A., McGregor, S., & Jin, F. (2010). Wind Effects on Past and Future Regional Sea Level Trends in the Southern Indo-Pacific. *Journal of Climate*, *23*(16), 4429–4437. https://doi.org/10.1175/2010JCLI3519.1Tozer, B., Sandwell, D. T., Smith, W. H. F., Olson, C., Beale, J. R., & Wessel, P. (2019). Global Bathymetry and Topography at 15 Arc Sec: SRTM15+. *Earth and Space Science*, *6*(10), 1847–1864. https://doi.org/10.1029/2019EA000658Tsimplis, M. N., Calafat, F. M., Marcos, M., Jordà, G., Gomis, D., Fenoglio-Marc, L., et al. (2013). The effect of the NAO on sea level and on mass changes in the Mediterranean Sea. *Journal of Geophysical Research: Oceans*, *118*(2), 944–952. https://doi.org/10.1002/jgrc.20078Vejmelka, M., Pokorná, L., Hlinka, J., Hartman, D., Jajcay, N., & Paluš, M. (2015). Non-random correlation structures and dimensionality reduction in multivariate climate data. *Climate Dynamics*, *44*(9), 2663–2682. https://doi.org/10.1007/s00382-014-2244-zVinogradova, N. T., Ponte, R. M., & Stammer, D. (2007). Relation between sea level and bottom pressure and the vertical dependence of oceanic variability. *Geophysical Research Letters*, *34*(3). https://doi.org/10.1029/2006GL028588Volkov, D. L., & Landerer, F. W. (2013). Nonseasonal fluctuations of the Arctic Ocean mass observed by the GRACE satellites. *Journal of Geophysical Research: Oceans*, *118*(12), 6451–6460. https://doi.org/10.1002/2013JC009341Volkov, D. L., Lee, S., Landerer, F. W., & Lumpkin, R. (2017). Decade-long deep-ocean warming detected in the subtropical South Pacific. *Geophysical Research Letters*, *44*(2), 927–936. https://doi.org/10.1002/2016GL071661Volkov, D. L., Baringer, M., Smeed, D., Johns, W., & Landerer, F. W. (2019). Teleconnection between the Atlantic Meridional Overturning Circulation and Sea Level in the Mediterranean Sea. *Journal of Climate*, *32*(3), 935–955. https://doi.org/10.1175/JCLI-D-18-0474.1Wang, Z., Hamilton, J., & Su, J. (2017). Variations in freshwater pathways from the Arctic Ocean into the North Atlantic Ocean. *Progress in Oceanography*, *155*, 54–73. https://doi.org/10.1016/j.pocean.2017.05.012Watkins, M. M., Wiese, D. N., Yuan, D., Boening, C., & Landerer, F. W. (2015). Improved methods for observing Earth's time variable mass distribution with GRACE using spherical cap mascons. *Journal of Geophysical Research: Solid Earth*, *120*(4), 2648–2671. https://doi.org/10.1002/2014JB011547Wiese, D. N., Landerer, F. W., & Watkins, M. M. (2016). Quantifying and reducing leakage errors in the JPL RL05M GRACE mascon solution. *Water Resources Research*, *52*(9), 7490–7502. https://doi.org/10.1002/2016WR019344Willebrand, J., Philander, S. G. H., & Pacanowski, R. C. (1980). The Oceanic Response to Large-Scale Atmospheric Disturbances. *Journal of Physical Oceanography*, *10*(3), 411–429. https://doi.org/10.1175/1520-0485(1980)010<0411:TORTLS>2.0.CO;2